Nonaffine behavior of three-dimensional semiflexible polymer networks

Hamed Hatami-Marbini

Phys. Rev. E **93**, 042503 — Published 22 April 2016

DOI: 10.1103/PhysRevE.93.042503

Non-affine behavior of three-dimensional semiflexible polymer networks

Hamed Hatami-Marbini[1]

Department of Mechanical & Industrial Engineering, University of Illinois at Chicago, Chicago, IL 60607

ABSTRACT

Three-dimensional semiflexible polymer networks are the structural building block of various biological and structural materials. Previous studies have primarily used two-dimensional models for understanding the behavior of these networks. In this work, we develop a three-dimensional non-affinity measure capable of providing direct comparison with continuum level homogenized quantities, i.e. strain field. The proposed non-affinity measure is capable of capturing possible anisotropic microstructure of the filamentous networks. This strain-based non-affinity measure is used to probe the mechanical behavior at different length scales and investigate the effects of network mechanical and microstructural properties. Specifically, it is found that while all non-affinity measure components have a power-law variation with the probing length scale, the degree of non-affinity decreases with increasing the length scale of observation. Furthermore, the amount of non-affinity is a function of network fiber density, bending stiffness of the constituent filaments, and the network architecture. Finally, it is found that the two power-law scaling regimes previously reported for two-dimensional systems do not appear in three-dimensional networks. Also, unlike two-dimensional models, the exponent of the power law relation depends weakly on the density of the three-dimensional networks.

I. INTRODUCTION

[1] Email: hatami@uic.edu, hamed.hatami@gmail.com

There exists a large number of structural and biological materials whose microstructure appears as an interconnected network of randomly oriented filaments. Paper, felt, networks of carbon nanotubes are among structural materials and cytoskeleton and extracellular matrix of soft tissue are examples of biological materials [1-3]. For example, the cytoskeleton, an intertwined semiflexible filamentous network, provides the structural integrity of cells while contributing to the cellular functions such as division and migration [4-6]. Due to their preponderance and striking properties, semiflexible polymer networks have been the subject of much research over the past decades [2,3,7]. These filamentous structures are usually three-dimensional; nevertheless, many of previous studies are focused on two-dimensional random fiber networks because three-dimensional simulations are computationally challenging. The mechanical response of two- and three-dimensional networks is expected to be significantly different: two-dimensional networks (often simulated by depositing randomly oriented fibers on plane) correspond to the isostatic threshold; nevertheless, three-dimensional networks are sub-isostatic and are likely to have bending dominated non-affine response.

The mechanical behavior of filament-based network structures depends not only on the mechanical properties of individual constitutes but also on their microstructure. It is well-known that the deformation of disordered systems including random fiber networks when subjected to a uniform far-field loading is non-affine, i.e., the local strain field is not homogeneous. The non-affine deformation allows a system to accommodate the applied deformation at a lower overall energy level compared to the energy that is expected from the affine assumption. Di-Donna and Lubensky used the correlation function of non-affine displacement components in order to investigate the degree of non-affinity in disordered domains [8]. They showed that while the spatial correlation function varies logarithmically with distance in two-dimension, it varies

inversely with distance in three-dimension. The degree of non-affinity of randomly crosslinked fibrous networks has been widely studied in two-dimension [9-16]. For example, Langer and Liu [17] quantified the non-affinity as the root mean square of the difference between the actual and affine displacement of all crosslinks. Head et al. [14] and Bai et al. [16] characterized non-affinity using a two-point scalar measure, i.e. calculating the change in orientation of a vector between two nodes due to deformation. Onck et al. [11] used a similar scalar measure which is defined as the difference between affine and non-affine nodal displacement divided by the position vector of the respective node. Moreover, Hatami-Marbini and Picu [13] developed a two-dimensional measure of non-affinity. These previous studies have shown that the response of two-dimensional networks becomes more non-affine with decreasing the fiber number density and decreasing the rigidity of the fibrous constituents. Based on these observations, a new length scale in terms of the flexibility of the filaments and mean segment length of the network is defined to distinguish between affinely and non-affinely deformed two-dimensional networks [9,14]. It yet remains to be determined how well the above findings, pertinent to two-dimensional models, could represent the properties of three-dimensional filamentous networks.

The elastic properties of three-dimensional systems have also been investigated [18-23]. Because of the architecture and coordination number of these networks, the bending of filaments is expected to be significant. Thus, non-affine bending deformation is anticipated to play a more dominant role. The simulations by Huisman and Lubensky [18] supports this intuitive hypothesis and characterize non-affine bending-dominated elasticity of three-dimensional networks. Nevertheless, three dimensional lattice-based fiber network models, i.e. Phantom and generalized Kagome networks, suggest a crossover from the bending-dominated to the stretch-dominated response [20,21].

The present work investigates the mechanical properties of three-dimensional networks in a systematic way by creating a new strain-based three dimensional non-affinity measure. This non-affinity parameter is used to determine the influence of network geometric properties and constituents' material properties on degree of non-affinity of three-dimensional fibrous networks. Since this new measure of non-affinity characterizes the strain distribution in three-dimensional filamentous structures at different length scales, it provides necessary information for developing stochastic method to determine their "homogenized" mechanics [24]. Similar to two-dimensional fiber networks, we find a power-law variation of all non-affinity measure components with the probing length scale for a wide range of length scales. Nevertheless, we report that the two power-law scaling regimes previously reported for two-dimensional systems do not appear in three-dimensional networks. We also show that similar to previous experimental data [12], the exponent of the existing power-law relation depends on the characteristic length scales of the networks. Finally, we show that the proposed non-affinity measure is able to capture the dependence of the non-affine response on the fiber network architecture.

II. THE MODEL

Although real networks are composed of filaments with complex geometry, three-dimensional crosslinked networks in the present study are created by placing N straight fibers of length L_0 of random orientation in a cubic region of size L^3. All fibers are assumed to have a circular cross-section with radius r and length L_0. The shortest distance between each individual fibers is determined and a rigid permanent crosslink is defined between two fibers that are closer than a critical distance $L_{crs} / L_0 = 0.02$. It is noted that this critical distance affects the distribution function of segment lengths. In the present study, the excluded volume effects are not considered. Furthermore, although the natural three-dimensional networks are usually composed

of filaments embedded in a solvent, we solely focus on the properties of the filamentous network in this work and ignore the network-solvent interaction [25]. In other words, we only seek to characterize the non-affinity of three-dimensional networks in terms of their architecture, fiber density, and elastic moduli of their individual filaments. Furthermore, we characterize the behavior of systems subjected to infinitesimal deformation in order to avoid nonlinear effects. Using the above assumptions, we write the energy of a three-dimensional filament at zero temperature as [26]

$$U_f = \frac{1}{2}\int \mu \left(dl/ds\right)^2 ds + \frac{1}{2}\int \kappa_w \left(d^2v/ds^2\right)^2 ds + \frac{1}{2}\int \kappa_v \left(d^2w/ds^2\right)^2 ds + \frac{1}{2}\int \kappa_\phi \left(d\phi/ds\right)^2 ds \quad (1)$$

where s is the arc-length, dl/ds is the relative change in length, v and w are transverse displacements, ϕ is the angle of rotation, κ_w and κ_v are bending moduli, κ_ϕ is the torsional modulus, and μ is the stretching modulus. For an athermal filament with circular cross-section, the bending and torsional moduli are of the same order, i.e. $\kappa = \kappa_w \sim \kappa_v \sim \kappa_\phi \propto E_f r^4$ and the stretching modulus is given by $\mu \propto E_f r^2$ where E_f is the Young's modulus of the individual filaments. It is noted that, although not studied here, the model can consider the thermal fluctuations by letting μ and κ be independent of each other [14]. Furthermore, it is noted that, similar to the observation of Zager et al. [22], we find that the torsional energy contribution is smaller than the bending energy contribution.

The total energy of the network subjected to displacement boundary condition is written using Equation (1) and the solution (deformation of the nodes) is found by minimizing this total energy. Once the response of the system is obtained, the strain field (deformation gradients) at different probing length scales is computed by extending the two-dimensional strain gage based

rosette tensometry method to the three-dimension [13]. In three dimension, the strain matrix is fully determined by measuring the normal strain in six different directions. Briefly, consider six virtual strain gages with arbitrary unit directions, $\mathbf{n}^{(i)}$, $i=1..6$, which forms a tetrahedron. The normal strain in the i^{th} strain gage is represented by $\boldsymbol{\varepsilon}^{\mathbf{n}^{(i)}}=\left(\varepsilon_1^{\mathbf{n}^{(i)}} \quad \varepsilon_2^{\mathbf{n}^{(i)}} \quad \varepsilon_3^{\mathbf{n}^{(i)}}\right)$ where

$$\varepsilon_j^{\mathbf{n}^{(i)}}=\sum_{k=1}^{3} n_k^{(i)}\varepsilon_{jk}, j=1..3 \text{ and } i=1..6. \quad (2)$$

For each tetrahedron, $\varepsilon^{\mathbf{n}^{(i)}}$ and $\mathbf{n}^{(i)}$ are known. Therefore, a linear system of equations can be formed and solved for strain components ε_{jk}, $j,k=1..3$, which are equal to the deformation gradients $\left(\partial u_j/\partial x_k+\partial u_k/\partial x_j\right)/2$.

Here, sextuplets of nodes are first selected such that they form approximately an equilateral tetrahedron of edge size a. The normal strain along each side of the tetrahedron (virtual strain gage) is calculated from the nodal displacement. This strain value can be considered as the mean normal strain $\varepsilon^{\mathbf{n}^{(i)}}=\frac{1}{a}\int_a \varepsilon^{\mathbf{n}^{(i)}}(a)\,da$ over the length of the i^{th} virtual strain gage. Moreover, the calculated strain matrix for each tetrahedron can be considered as the average non-affine strain field $\boldsymbol{\varepsilon}^{\text{na}}=\left\langle\varepsilon_{jk}^{\text{na}}\right\rangle_l=\frac{1}{V}\int_V \varepsilon_{jk}dV$ over the length scale l proportional to the volume $V=a^3/6\sqrt{2}$ of the tetrahedron, i.e. $l\sim a$. The corresponding affine strain components $\boldsymbol{\varepsilon}^{\text{af}}$ are calculated from the affine estimate of the nodal displacement. It is noted that the affine strain matrix is equal to the applied far-field uniform strain at all length scales l. The 3D non-affinity strain-based measure matrix $\mathbb{N}(l)$ is defined as the fluctuation of the actual strain components (deformation gradients) relative to their affine estimates, i.e.

$$\mathbb{N}(l) = \eta_{jk} = \left\langle \left(\varepsilon_{jk}^{\mathrm{af}} - \varepsilon_{jk}^{\mathrm{na}} \right)^2 \right\rangle_l \Big/ \left(\varepsilon^{\mathrm{ap}} \right)^2 , j,k=1..3, \quad (3)$$

where $\varepsilon^{\mathrm{ap}}$ is the applied far-field strain. The above strain-based non-affinity measure is independent of the applied far-field loading and gives the average of the displacement gradients over length scale *l*. Thus, in addition to being useful for investigating the effect of characteristic length scale on the non-affine response of the three-dimensional networks, it is very well-suited for investigating the "homogenized" mechanics of these networks at different length scales.

The mechanical properties, i.e. stretching, bending, and torsional stiffness, of the cylindrical filaments are expressed in terms their radius and Young's modulus. If the stretching modulus is used for normalization, a new characteristic length scale $l_b = \sqrt{\kappa/\mu} \propto r$ results. Another length scale is the mean segment length l_c which distinguishes between densely or sparsely crosslinked filamentous networks. In addition to the characteristic length scales l_c and l_b, the length of filaments L_0 and the size of the simulation box L may play a role. In this work, L_0 is used to normalize all the length scales and filamentous networks with L/L_0 from 2 to 10, l_b/L_0 from 10^{-3} and 10^0, and l_c/L_0 from 0.025 (~N=3200) to 0.25 (~N=200) are considered.

In order to investigate the possible influence of the network architecture on its non-affine behavior, networks with preferential fiber orientation are generated and their behavior is compared with those made up of uniformly distributed filaments [27]. The orientation tensor is used to quantify the preferential orientation of the filaments [28]. This tensor is computed by averaging the dyadic product of the orientation of all fibers, i.e.

$$\begin{aligned} O_{mn} &= \left\langle \alpha_m^{(i)} \alpha_n^{(i)} \right\rangle, \quad m,n = 1..3 \\ \boldsymbol{\alpha}^{(i)} &= \begin{pmatrix} \sin\theta\cos\phi & \sin\theta\sin\phi & \cos\theta \end{pmatrix} \end{aligned}, \quad (4)$$

where θ and ϕ are, respectively, polar and azimuthal angles, and $\boldsymbol{\alpha}^{(i)}$ is the orientation vector of the i^{th} filament in the 3D space. For networks with uniform distribution of fiber orientation, the orientation tensor is given by $O_{11} = O_{22} = O_{22} = 1/3,$ and $O_{12} = O_{13} = O_{23} = 0$.

III. RESULTS

Figure 1 plots the components of the non-affinity measure as a function of probing length scale l for three dimensional filamentous networks with a fiber number density of N=200 and $l_b/L_0=10^{-3}$ when subjected to a uniform strain $\varepsilon^{ap} = \varepsilon_{11}$ in the x_1 direction. All non-affinity measure components exhibit a power law scaling with the probing length scale l. Similar power law behavior is observed for all other networks; nonetheless, characteristic length scales of the networks affect the amount of non-affinity and the exponent of the power law relation (as discussed below). The presence of the power-law relation for the non-affinity measure (which is defined in terms of the fluctuations of the strain field) implies that there is no characteristic length scale over which the affine mechanical response could be separated from the non-affine behavior for three dimensional filamentous networks. In the following, we investigate the effects of density of the system (as measured by l_c/L_0), the elasticity of the individual filaments (as measured by l_b/L_0), and the filament preferential orientation (as measured by O_{ij}) on the non-affine behavior.

The influence of characteristic length scale l_b on non-affine behavior of three dimensional fiber networks is shown in Figure 2. In this plot, the first component of the non-affinity measure is plotted for systems of fiber number density N=200 (l_c/L_0~0.25) and $l_b/L_0 = 10^{-3}$ to 10^{0}. With increasing the parameter l_b (the bending stiffness of filaments), the amount of non-affinity decreases but becomes almost insensitive to this parameter for large values of l_b/L_0. The effect of

mean fiber length segment on the first component of the non-affinity is plotted in Figure 3. In this plot, three-dimensional networks with fiber number density of 200 to 3200 per unit volume (l_c/L_0~0.025 to 0.25) and l_b/L_0= 0.01 are subjected to uniform far-field uniaxial extension. It is seen that with increasing fiber number density (i.e. decreasing mean segment length), the behavior of the network becomes more affine. Figure 3 shows that the amount of non-affinity seems to saturate with increasing fiber number density, i.e. the non-affinity measure becomes less dependent on the fiber density when N > 1600. It is also seen that the scaling exponent of the power-law relation decreases with increasing the fiber number density, see inset of Figure 3. A similar trend is seen with increasing the bending rigidity of the filaments. This is an important observation which does not appear in the analysis of two-dimensional filamentous networks [13] but agrees with experimental data obtained on F-actin networks [12]. Liu et al. used tracking embedded probe particles to find the local strain field of F-actin networks experimentally. They then characterized the degree of non-affinity at a length scale r as $\langle r^2\Delta\theta^2\rangle_r/\gamma^2$ where $\Delta\theta$ is the change of angle of two particles separated by distance r and γ is the applied shear strain. They observed that with increasing the crosslink density (decreasing mean segment length l_c), the non-affinity is independent of applied strain γ, its magnitude decreases, and the exponent of the power-law increases. The present three-dimensional model captures all these experimental observations. Therefore, Liu et al.'s experimental measurements can be used a promising validation study for the present numerical simulations. It needs to be mentioned that the numerical results for dense systems (N>1600) are obtained from a smaller simulation box (L/L_0~*2*). This prevented us from obtaining the amount of non-affinity at large probing length scales and is a limitation of the present study. This limitation might have also affected the

reported variation of the scaling exponent with density (inset of Figure 3) because of the size effect problem.

Although non-affinity is more significant for systems with low density and/or less stiff filaments, Figures 2-3, the two power-law scaling regimes previously reported for two-dimensional systems [13,14,16] is absent in three-dimensional networks (within the range of parameters considered here). In Figure 4, the first component of non-affinity measure is plotted for two- and three-dimensional networks of similar fiber number density N=150, 400, and 800. This plot shows that scaling exponent of the power-law behavior of three-dimensional networks is within the range of previously reported larger scaling exponents (1.65±0.05) for two-dimensional fiber networks. Nevertheless, the power-law scaling regime with the smaller scaling exponent (0.42±0.03) does not appear. The reason for this could be the fundamental difference between isostacity of two- and three-dimensional networks. In two-dimensional isostatic fiber networks, the scaling behavior changes at length scales smaller than a characteristic length scale $r^*/L_0 \approx 0.5$ (Figure 4). This is because when the bending stiffness of the filaments increases, their contiguity becomes significant and the fiber segments behave similar to the element of a truss with central forces (stretching deformation). Nonetheless, three-dimensional networks with binary crosslinks have a connectivity well below iso-staticity and their behavior is bending dominated. Therefore, although the exponent reduces for dense three-dimensional fiber networks or those composed of fiber with higher bending rigidity, the connectivity of the structure is not enough (at least within the range of parameters of the present study) to cause the behavior of the network to become similar to that of the two-dimensional networks. This difference in the behavior of two- and three-dimensional networks is expected to be very important because an accurate

characterization of the scaling properties is a necessary step for developing stochastic methods that can be used to solve boundary value problems on three-dimensional fiber networks [24].

Parenthetically, a note is in place regarding previous studies on two-dimensional networks which showed that there exists a non-affinity length scale $\lambda = \lambda(l_b, l_c)$ characterizing the transition from affine to non-affine response. This parameter has been expressed as $\lambda = l_c(l_c/l_b)^z$ where z is a constant equal to 1/4, 1/3, and 2/5 based on mean field theories, numerical simulations, and, scaling arguments, respectively. Following Head et al.[9], we will use z=1/3 in order to calculate the non-affinity measure for the plots shown in Figure 4. For two-dimensional networks with N=150, 400, and 800, L_0/λ is equal to 2, 46, and 115 while it is much lower for the corresponding three-dimensional networks, i.e. 0.9, 2.2, 4.7, respectively. It is first noted that this length scale does not determine the existence of the single or two scaling regimes (it has been shown that the bending stiffness of the fibers, in two-dimensional networks, controls the scaling at the small length scale, see reference [13]). Furthermore, the three-dimensional networks may have a different form of $\lambda = \lambda(l_b, l_c)$. Nevertheless, the significantly lower values of L_0/λ for three-dimensional networks compared to two-dimensional systems shown in Figure 4 is consistent with the observation that their behavior is more non-affine.

It is noted although three-dimensional networks has one scaling regime, their mechanical behavior can still transition from non-affine bending dominated deformation to affine stretching regime depending on the degree of non-affinity measure. In order to check this, the solution of the networks subjected to affine deformation is obtained and is used to calculate the effective elasticity of the networks at length $l=L$ or $l/L=1$. The affine uniaxial tension causes stretching and rotation of the fibers; thus, the behavior is dominated by only stretching modes. In Figure 5,

the ratio of the non-affine and affine energy estimates for networks with different fiber number density is plotted as a function of characteristic length l_b/L_0. It is seen that this ratio approaches one with increasing l_b/L_0 and the system tries to accommodate the applied deformation by stretching of the filaments. This is because the bending of filaments gets very costly as $l_b \to \infty$. On the hand, the behavior of the networks is dominated by bending of filaments at small l_b/L_0 because the stretching of the filaments requires more energy than their bending. For networks with fixed l_b/L_0, a similar behavior is expected as $l_c \to 0$. Despite the above discussion, special attention should be paid to the fact that three-dimensional networks with binary crosslinks are far from the critical Maxwell's coordination number (connectivity); therefore, their stability is dependent on bending elasticity of filaments. In other words, the very large energetic cost of filaments does not necessarily inhibit these modes of deformation especially if they are required for the overall stability of the structure. This topic and the specific form of non-affinity length scale $\lambda = \lambda(l_b, l_c)$ are currently under study and the findings will be reported in a separate publication.

In addition to the dependence of the non-affinity on fiber number density (represented by l_c), fiber properties (denoted by l_b), the network architecture is also expected to affect the non-affine behavior of randomly crosslinked networks. In order to investigate the possible influence of network architecture on the non-affinity, we generated networks with preferential fiber orientation and studied their non-affine repose, Figure 6. In this plot, the fiber number density and fiber material properties are kept constant and three types of network architecture are considered: random, semi-random, and preferentially oriented. The average non-zero components of the orientation tensor for these networks are $\left(O_{11} = O_{22} = O_{22} = 0.33\right)$,

$\left(O_{11} = O_{22} = 0.49,\ O_{33} = 0.02\right)$, and $\left(O_{11} = O_{22} = 0.50\right)$, respectively. Figure 6c shows that while the network architecture has limited influence on the power-law variation of the non-affinity measure with the probing length scale, it significantly changes the amount of non-affinity. As the networks become more preferentially oriented, both non-affinity components η_{11} and η_{33} increase. Nevertheless, the increase in η_{11} is much less than η_{33} component, which is expected considering the microstructure of the networks. The increase in η_{11} can be explained as following: the filaments in preferentially orientated networks are primarily arranged in parallel x_1- x_2 plane with few fibers in x_3 –direction (Figure 6b). Therefore, when loaded in x_1-direction, the stacks of filaments in x_1- x_3 plane slide with respect to each other and cause an increase in non-affinity. On the other hand, when filaments are uniformly deposited in all directions, a sturdier structure is formed to resist the applied force and a more affine response is expected.

Another interesting observation is that while the line representing η_{33} lies below the line for η_{11} at all probing length scales, η_{33} component becomes larger than the η_{11} component when the networks become preferentially oriented. This can be explained by based on the network architecture. For the networks whose fibers are uniformly distributed, the applied strain in the x_1-direction causes the filaments to become preferentially oriented in this direction. Therefore, $\eta_{11} > \eta_{33}$, i.e. the behavior is more affine in the direction of the applied load. Nevertheless, for networks called "preferentially oriented" in Figure 6, prior to the application of the external load, the fibers (as seen in x_1- x_3 plane, Figure 6b) are preferentially oriented in the x_1 direction. Therefore, when these structures are subjected to uniaxial tensile strain $\varepsilon^{\mathrm{ap}} = \varepsilon_{11}$, it is easier for the filaments to move in the x_3-direction, i.e. the behavior is more non-affine in this direction ($\eta_{33} > \eta_{11}$). This discussion implies that the proposed non-affinity measure is able to capture the

possible anisotropy in the architecture of the fiber networks. This is important as it shows the potential application of the proposed non-affinity measure in inferring the microstructural information from displacement field measurements. Other non-affinity measures do not often have this capability. For example, consider one of the commonly-used scalar non-affinity measures defined as [8,14,17,20]

$$\Gamma = \frac{1}{\left(l_c \varepsilon^{ap}\right)^2} \left\langle \left(u_i - u_i^a\right)\left(u_i - u_i^a\right) \right\rangle \quad (5)$$

where u_i denotes the i^{th} displacement component of a crosslink and u_i^a represents its affine estimate. Using this non-affinity measure, we obtain $\Gamma \approx 82$, 91, and 120 for networks called random, semi-random, and preferentially oriented in Figure 6. This measure, too, show that as the networks become preferentially oriented, their behavior becomes more non-affine (which agrees with the observed increase in the non-affinity components). Nevertheless, it is unable to provide any insight on the underlying cause of such an increase.

IV. CONCLUSION

In conclusion, it is shown here that mechanical response of three-dimensional networks is non-affine at all length scale and their deformation is never exactly affine. Furthermore, it is found that the non-affinity strain components decay with distance following a power-law relation. Unlike two-dimensional networks, the strain-based non-affinity measure only shows one scaling regime and the exponent of the power law scaling is dependent on the characteristic length scales. In particular, the scaling exponent decreases with increasing the fiber number density as it

was observed previously in experimental measurements. It is noted that increasing the bending stiffness of the filaments and fiber number density reduce the amount of non-affinity and cause the overall behavior becomes more affine. The network architecture does not significantly affect the power of the power-law variation of the non-affinity measure with the probing length scale; nevertheless, it significantly affect the amount of non-affinity. The proposed non-affinity measure can be used to infer microstructural information of random fiber networks and similar systems from displacement field measurements.

ACKNOWLEDGMENTS

The author would like to acknowledge the support in part by National Science Foundation under Grant No. 1351461.

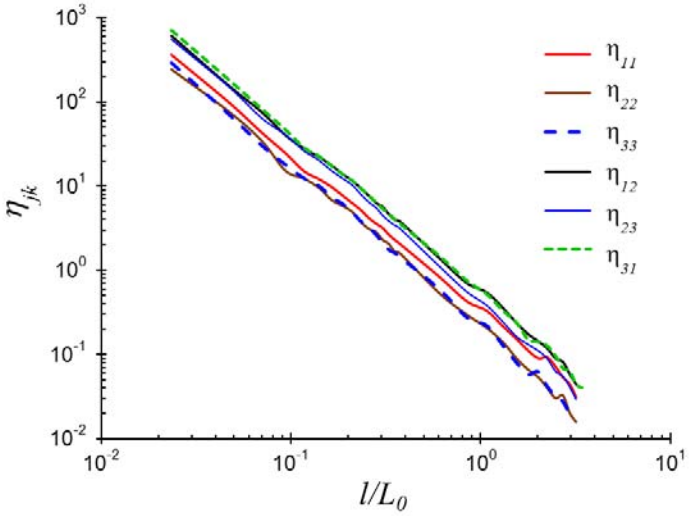

Figure 1. The variation of normalized non-affinity components η_{jk}, *j,k=1,2,3* as a function of normalized probing length scale for networks with fiber number density N=200 and l_b/L_0=0.001 when subjected to uniaxial tensile strain $\varepsilon^{ap} = \varepsilon_{11}$

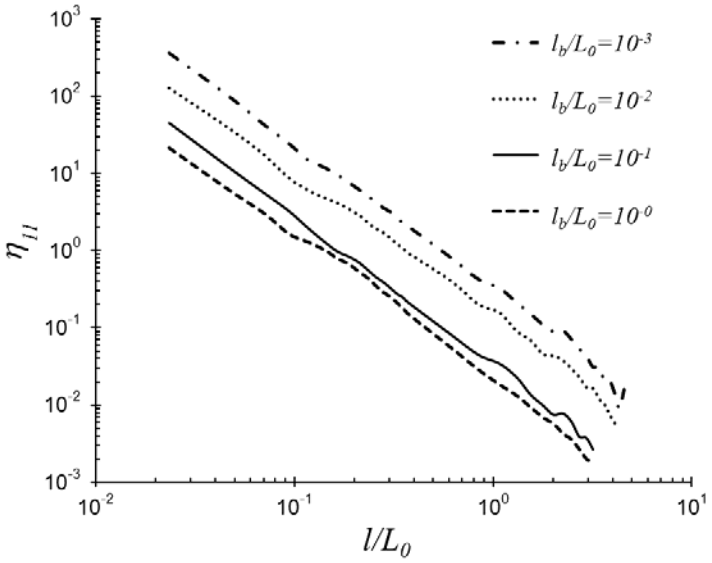

Figure 2. The variation of the first component of the normalized non-affinity components η_{11} as a function of the normalized probing length scale for networks composed of fibers with different flexibility parameter l_b/L_0 and N=200, when subjected to uniaxial tensile strain $\varepsilon^{ap} = \varepsilon_{11}$

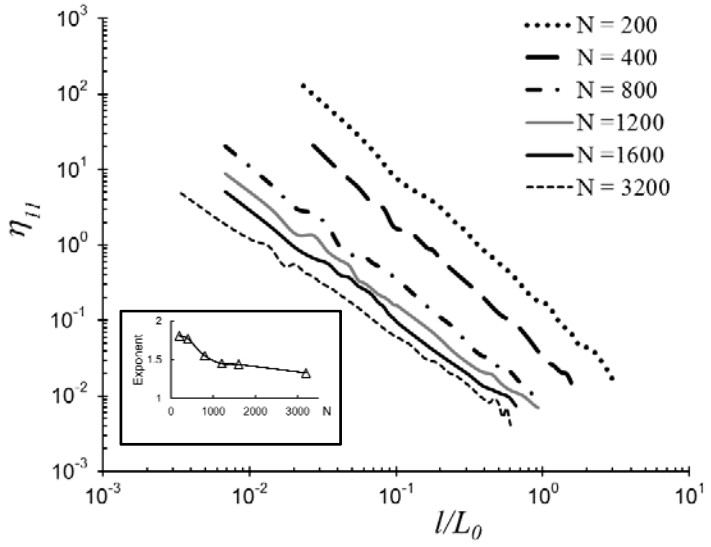

Figure 3. The variation of the first component of the normalized non-affinity components η_{11} as a function of the normalized probing length scale for networks with $l_b/L_0 = 0.01$ and different fiber number densities N, when subjected to uniaxial tensile strain $\varepsilon^{ap} = \varepsilon_{11}$. The inset shows the variation of the exponent of the power law scaling as a function of N.

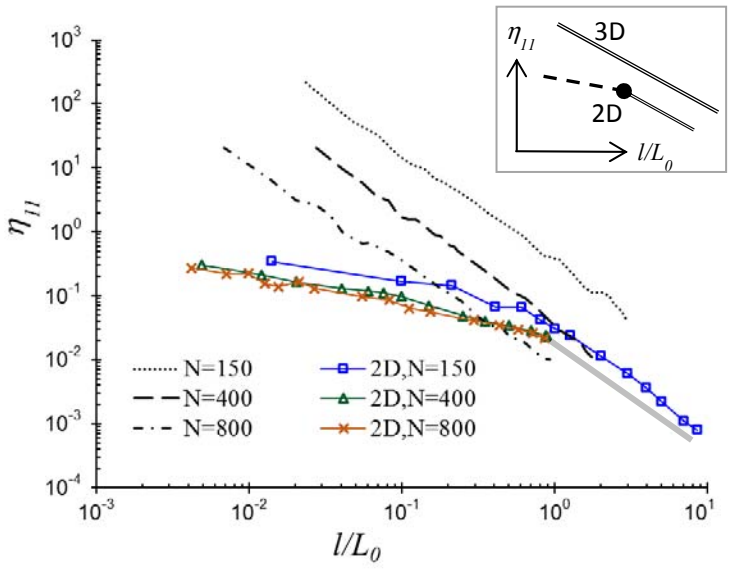

Figure 4. The first component of non-affinity η_{11} as a function of the normalized probing length scale for two-dimensional and three-dimensional networks with $l_b/L_0 = 0.01$ and different fiber number densities N, when subjected to uniaxial tensile strain $\varepsilon^{ap} = \varepsilon_{11}$. It is seen that the scaling regime with small exponent does not appear in three-dimensional networks. Moreover, at a given fiber number density, three-dimensional systems show significantly more non-affine behavior that their respective two-dimensional networks.

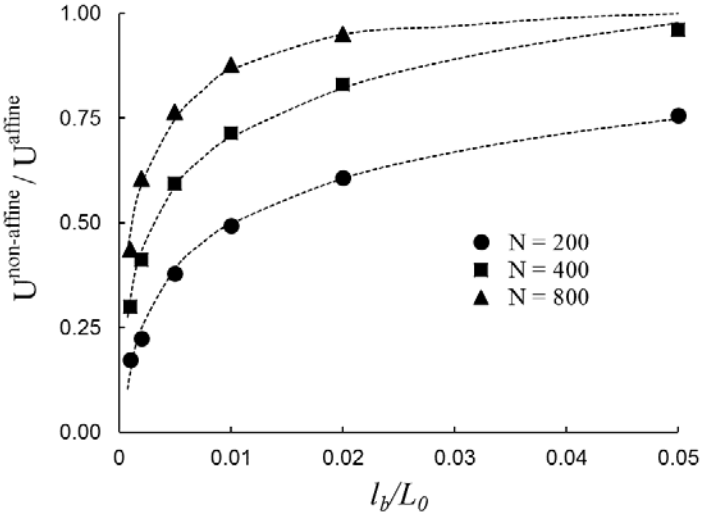

Figure 5. The influence of filament flexibility l_b/L_0 on the ratio of non-affine and affine total energy $U^{non\text{-}affine}/U^{affine}$ of the three-dimensional networks with different fiber number density, when the network is subjected to uniaxial tensile strain $\varepsilon^{ap} = \varepsilon_{11}$

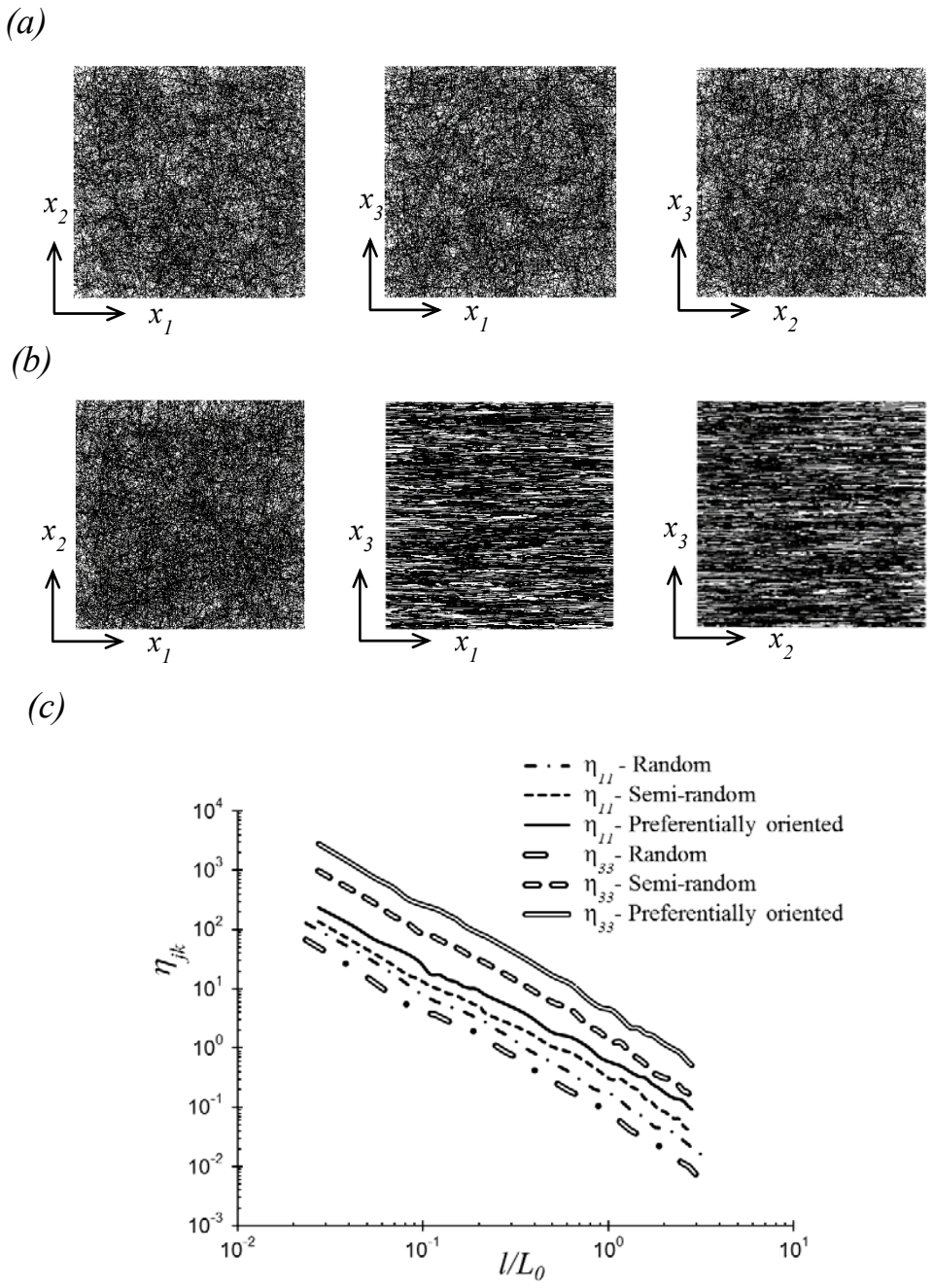

Figure 6. The influence of fiber network microstructure on the first (η_{11}) and third (η_{33}) component of the normalized non-affinity measure for networks with l_b/L_0 = 0.01 and N=200 when subjected to uniaxial tensile strain $\varepsilon^{ap} = \varepsilon_{11}$. Three types of network architecture is considered: random, semi-random, and preferentially oriented. The representative microstructure of (a) random networks and (b) preferentially oriented networks is shown. (c) As the networks become preferentially oriented the non-affinity increases but the exponent of the power-law relation remains unaltered. The ratio of first (η_{11}) and third (η_{33}) non-affinity component is related to the degree of anisotropy as discussed in the text.

References

[1] L. J. Gibson and M. F. Ashby, *Cellular solids: structure and properties* (Cambridge university press, 1997).

[2] R. Picu, Soft Matter **7**, 6768 (2011).

[3] C. P. Broedersz and F. C. MacKintosh, Reviews of Modern Physics **86**, 995 (2014).

[4] H. Hatami-Marbini and M. R. Mofrad, in *Complex Fluids in Biological Systems* (Springer, 2015), pp. 187.

[5] H. Hatami-Marbini and M. R. Mofrad, in *Cellular and Biomolecular Mechanics and Mechanobiology* (Springer, 2011), pp. 3.

[6] B. Alberts, A. Johnson, J. Lewis, M. Raff, K. Roberts, and P. Walter, *Molecular Biology of the Cell* (Garland Science, New York, 1994).

[7] H. Hatami-Marbini and C. Picu, in *Advances in Soft Matter Mechanics* (Springer Berlin Heidelberg, 2012), pp. 119.

[8] B. DiDonna and T. Lubensky, Physical Review E **72**, 066619 (2005).

[9] D. A. Head, A. J. Levine, and F. MacKintosh, Physical review letters **91**, 108102 (2003).

[10] J. Wilhelm and E. Frey, Physical review letters **91**, 108103 (2003).

[11] P. Onck, T. Koeman, T. Van Dillen, and E. Van der Giessen, Physical review letters **95**, 178102 (2005).

[12] J. Liu, G. Koenderink, K. Kasza, F. MacKintosh, and D. Weitz, Physical review letters **98**, 198304 (2007).

[13] H. Hatami-Marbini and R. Picu, Physical Review E **77**, 062103 (2008).

[14] D. A. Head, A. J. Levine, and F. C. MacKintosh, Physical Review E **68**, 061907 (2003).

[15] P. L. Chandran and V. H. Barocas, Journal of biomechanical engineering **128**, 259 (2006).

[16] M. Bai, A. R. Missel, W. S. Kluga, and A. J. Levine, Soft Matter **7**, 907 (2010).

[17] S. A. Langer and A. J. Liu, The Journal of Physical Chemistry B **101**, 8667 (1997).

[18] E. Huisman and T. C. Lubensky, Physical review letters **106**, 088301 (2011).

[19] E. Huisman, T. Van Dillen, P. Onck, and E. Van der Giessen, Physical review letters **99**, 208103 (2007).

[20] C. Broedersz, M. Sheinman, and F. MacKintosh, Physical review letters **108**, 078102 (2012).

[21] O. Stenull and T. Lubensky, arXiv preprint arXiv:1108.4328 (2011).

[22] G. Zagar, P. R. Onck, and E. Van der Giessen, Macromolecules **44**, 7026 (2011).

[23] G. Zagar, P. R. Onck, and E. van der Giessen, Biophysical journal **108**, 1470 (2015).

[24] H. Hatami-Marbini and R. C. Picu, Physical Review E **80**, 046703 (2009).

[25] L. Zhang, S. Lake, V. Barocas, M. Shephard, and R. Picu, Soft matter **9**, 6398 (2013).

[26] L. Landau and E. Lifshitz, *Theory of Elasticity* (Pergamon Press, Oxford, 1975).

[27] H. Hatami-Marbini and R. Picu, Acta mechanica **205**, 77 (2009).

[28] S. G. Advani and E. M. Sozer, *Process modeling in composites manufacturing* (CRC Press, 2010), Vol. 59.